Vibrational Circular Dichroism within the Polarizable Continuum Model: A Theoretical Evidence of Conformation Effects and Hydrogen Bonding for (*S*)-(−)-3-Butyn-2-ol in CCl_4 Solution

Chiara Cappelli,[†] Stefano Corni,[‡] Benedetta Mennucci,*[,†] Roberto Cammi,[§] and Jacopo Tomasi[†]

Dipartimento di Chimica e Chimica Industriale, Università di Pisa, via Risorgimento 35, 56126 Pisa, Italy, Scuola Normale Superiore, Piazza dei Cavalieri 7, 56126 Pisa, Italy, and Dipartimento di Chimica Generale ed Inorganica, Università di Parma, Parco Area delle Scienze 1, 43100 Parma, Italy

Received: May 22, 2002; In Final Form: September 11, 2002

Vibrational circular dichroism (VCD) and infrared (IR) spectra of (−)-3-butyn-2-ol in CCl_4 solution have been calculated within the framework of the polarizable continuum model (PCM). Density functional theory and gauge-invariant atomic orbitals are exploited in the quantum-mechanical approach, and nonequilibrium and local field effects are taken into account in the solvation model. The influence of both dielectric environment effects and H-bonding intermolecular interactions are analyzed and compared to the experimentally observed variations of the spectra at different concentrations of alcohol.

1. Introduction

This paper will treat the calculation of vibrational circular dichroism (VCD) spectra of (*S*)-3-butyn-2-ol in CCl_4 solution. This chemical is a useful material for different classes of compounds, such as drugs, agrochemicals, perfumes, and liquid crystals.[1]

Experimental IR and VCD spectra of (*S*)-3-butyn-2-ol in CCl_4 solution have been recently published by Wang and Polavarapu.[2] In that paper, which represents the first study in the literature dealing with the vibrational analysis of 3-butyn-2-ol, two main aspects are pointed out: (i) as the molecule exists in different conformations having comparable importance, the experimental IR and VCD spectra will be the superposition of the spectra of the single conformers; (ii) both IR and VCD spectra significantly change by changing the solute concentration. The two authors present a theoretical study for the isolated system, from which they try to explain the experimental findings; on the basis of their calculations, which do not take into account solvation and intermolecular interactions effects, they come to the conclusion that the differences in spectra going from dilute to concentrated solution depend on the change in the relative amount of the various conformations due to the occurrence of hydrogen bonding interactions between alcohol molecules.

Starting from Wang and Polavarapu paper, here we will perform calculations which consider that the system is not isolated, but immersed in CCl_4 solution, and that solute molecules can specifically interact through formation of H-bonded clusters. The theory of VCD calculations within the polarizable continuum model (PCM)[3] is presented here for the first time, even if a couple of PCM−VCD calculations have already been published.[4,5] Quantum mechanical computations of VCD intensities for isolated molecules are nowadays routinely performed (see, for example, ref 6 just to quote papers which appeared in the literature in the last couple of years) and exhibit an accuracy similar to that of other spectroscopic quantities. Less studied is the prediction of VCD spectra for solvated systems: in addition to the two already quoted articles,[4,5] only few other papers are present in the literature.[7] These resort to the simple Onsager continuum model to treat the solute−solvent electrostatic interaction.

Several recent developments have enormously enhanced the accuracy and efficiency of VCD calculations: among them are the implementation of direct analytical derivative methods,[8] the use[9,10] of gauge-invariant atomic orbitals (GIAOs),[11] and the development of hybrid density functionals for DFT calculations.[12] All these features will be used in the present work. Regarding the solvation model, effects due to a nonequilibrium solvent response to molecular vibrations, as well as to the so-called "local field" will be considered. Local field effects are of general occurrence when an external field interacts with a molecule in a condensed phase; they can be qualitatively defined as the effects arising from the fact that the field locally experienced by the molecule is different from the macroscopic (Maxwell) field in the medium.[13,14]

The concept of a solute solvent nonequilibrium system involves many different aspects related to the real nature of the solvent polarization: in a qualitative way, the polarization can be decomposed into different contributions each related to motions associated with the different degrees of freedom of the solvent molecules. The nonequilibrium assumption is that only the fast contributions are instantaneously equilibrated to the momentary molecular charge distribution whereas the slower terms cannot readjust, giving rise to an incomplete response of the solvent.[15]

The presentation will be organized as follows: in the next section we will discuss the theory of VCD spectra within the PCM including nonequilibrium and local field effects, then we will pass to the calculation of IR and VCD spectra of 3-butyn-2-ol. Calculated data will be compared with experimental findings at various concentrations, pointing out solvent effects and intermolecular H-bonding between solute molecules. In particular, we shall show that the effects due to the creation of large (possibly weakly bound) clusters can be qualitatively taken

[†] Università di Pisa.
[‡] Scuola Normale Superiore.
[§] Università di Parma.

10.1021/jp021273e CCC: $22.00
Published on Web 11/28/2002

into account through the modulation of the dielectric properties of the solution.

2. Theory

The differential response of a chiral sample to left and right circularly polarized light can be represented by the quantity $\Delta\epsilon$, defined as[16]

$$\Delta\epsilon = \epsilon_L - \epsilon_R \tag{1}$$

where $\epsilon_{L,R}$ are the molar absorption coefficients for left and right circularly polarized light, respectively. Ignoring for the moment solvent effects, the differential molar absorption coefficient at frequency ν, $\epsilon(\nu)$, is

$$\Delta\epsilon(\nu) = 4\gamma\nu\sum_i R_i f(\nu_i,\nu) \tag{2}$$

where ν_i is the frequency of the ith transition, γ is a numerical coefficient given, for example, in ref 16a, $f(\nu_i,\nu)$ the normalized line-shape function and

$$R_i = \mathrm{Im}[\langle 0|\boldsymbol{\mu}_{el}|1\rangle_i \cdot \langle 0|\boldsymbol{\mu}_{mag}|1\rangle_i] \tag{3}$$

the rotational strength. In eq 3, $\boldsymbol{\mu}_{el}$ and $\boldsymbol{\mu}_{mag}$ are the electric and magnetic dipole moment operators, respectively and $|0\rangle$, $|1\rangle$ are vibrational states. The transition moments in eq 3 may be written as

$$\langle 0|(\mu_{el})_\beta|1\rangle_i = \left(\frac{\hbar}{4\pi\nu_i}\right)^{1/2}\sum_{\lambda\alpha} S_{\lambda\alpha,i} P^\lambda_{\alpha\beta} \tag{4}$$

$$\langle 0|(\mu_{mag})_\beta|1\rangle_i = -(4\hbar^3\pi\nu_i)^{1/2}\sum_{\lambda\alpha} S_{\lambda\alpha,i} M^\lambda_{\alpha\beta} \tag{5}$$

where $P^\lambda_{\alpha\beta}$ and $M^\lambda_{\alpha\beta}$ are the atomic polar tensors (APTs) and atomic axial tensors (AATs), respectively, and the $S_{\lambda\alpha,i}$ matrix converts Cartesian displacement coordinates $X_{\lambda\alpha}$ of the nucleus λ to normal coordinates Q_i:

$$X_{\lambda\alpha} = \sum_i S_{\lambda\alpha,i} Q_i \tag{6}$$

ν_i and $S_{\lambda\alpha,i}$ are obtained simultaneously by diagonalization of the massweighted Cartesian force field (the Hessian). Within the double harmonic approximation, APTs and AATs of nucleus λ are defined by

$$P^\lambda_{\alpha\beta} = \left(\frac{\partial\langle\psi_g|(\mu^e_{el})_\beta|\psi_g\rangle}{\partial X_{\lambda\alpha}}\right)_{r_0} + Z_\lambda e\delta_{\alpha\beta} = 2\left\langle\left(\frac{\partial\psi_g}{\partial X_{\lambda\alpha}}\right)_{r_0}\middle|(\mu^e_{el})_\beta\middle|\psi_g\right\rangle + Z_\lambda e\delta_{\alpha\beta} \tag{7}$$

and

$$M^\lambda_{\alpha\beta} = I^\lambda_{\alpha\beta} + J^\lambda_{\alpha\beta} \tag{8}$$

with

$$I^\lambda_{\alpha\beta} = \left\langle\left(\frac{\partial\psi_g}{\partial X_{\lambda\alpha}}\right)_{R_0}\middle|\left(\frac{\partial\psi_g}{\partial B_\beta}\right)_{B_\beta=0}\right\rangle \tag{9}$$

$$J^\lambda_{\alpha\beta} = \frac{i}{4\hbar c}\sum_\gamma \epsilon_{\alpha\beta\gamma} r^0_{\lambda\gamma} Z_\lambda e \tag{10}$$

Here $\boldsymbol{\mu}^e_{el}$ is the electronic part of $\boldsymbol{\mu}_{el}$ and $Z_\lambda e$ and $\mathbf{r}^0_\lambda$ are the charge and position of nucleus λ at the equilibrium geometry $\mathbf{r}^0$, ψ_G is the wave function of the ground electronic state g, and $(\partial\psi_g/\partial X_{\lambda\alpha})$ and $(\partial\psi_g/\partial B_\beta)$ are the derivatives of the wave function of g with respect to nuclear displacement and magnetic field, respectively.

Let us stop to consider the calculation of $\Delta\epsilon$ for systems in solution.

In this paper, we will use the integral equation formalism (IEF)[17] version of the PCM to describe the solution. In this method, the solvent is modeled as a continuum, infinite, homogeneous and usually isotropic dielectric medium, characterized by a dielectric constant ϵ. The solute is hosted into a molecular-shaped cavity, and the electrostatic problem of the evaluation of the interaction energy between solute and solvent, including also mutual polarization effects, is solved by introducing an apparent charge distribution σ spread on the cavity surface. In computational practice, this continuous distribution is discretized in terms of point charges $\{q_i\}$, each associated with a small portion (tessera) of the cavity surface, and defined through a set of linear equations; in the PCM−IEF framework the expression to be used is

$$\mathbf{q} = -\mathbf{Q}\mathbf{V}^M \tag{11}$$

where $\mathbf{V}^M$ is a column vector containing the solute potential computed at the representative position of each tessera. $\mathbf{Q}$ is a square matrix with dimension equal to the number of tesserae, whose elements depend on geometrical cavity parameters and on the dielectric constant.[18]

The calculation of $\Delta\epsilon$ in the presence of a solvent medium still relies on eqs 2 and 3, but some refinements are needed. As already remarked in ref 19 with regard to infrared intensities for molecules in solution, the $\boldsymbol{\mu}_{el}$ operator in eq 3 has to be replaced by the sum of the dipole moment $\boldsymbol{\mu}_{el}$ of the molecule and the dipole moment $\boldsymbol{\mu}_{el}$ arising from the polarization induced by the molecule on the solvent. $\boldsymbol{\mu}_{el}$ takes into account effects due to the field generated from the solvent response to the probing field once the cavity has been created (the so-called "cavity field"). In principle also $\boldsymbol{\mu}_{mag}$ should be similarly reformulated. However, by assuming the response of the solvent to magnetic perturbations to be described only in terms of its magnetic permittivity (which is usually close to unity), it is reasonable to consider that the magnetic analogous of the electric "cavity field" gives minor contributions to R^{sol}_i. Thus, the final expression for R^{sol}_i to use is

$$R^{sol}_i = \mathrm{Im}[\langle 0|(\boldsymbol{\mu}_{el} + \tilde{\boldsymbol{\mu}}_{el})|1\rangle_i \cdot \langle 0|\boldsymbol{\mu}_{mag}|1\rangle_i] \tag{12}$$

and

$$\langle 0|(\mu_{el} + \tilde{\mu}_{el})_\beta|1\rangle_i = \left(\frac{\hbar}{4\pi\nu_i}\right)^{1/2}\sum_{\lambda\alpha} S^{sol}_{\lambda\alpha,i}((P^\lambda_{\alpha\beta})^{sol} + \tilde{P}^\lambda_{\alpha\beta}) \tag{13}$$

$$\langle 0|(\mu_{mag})_\beta|1\rangle_i = -(4\hbar^3\pi\nu_i)^{1/2}\sum_{\lambda\alpha} S^{sol}_{\lambda\alpha,i}(M^\lambda_{\alpha\beta})^{sol} \tag{14}$$

where the $S^{sol}_{\lambda\alpha,i}$ matrix is obtained by diagonalizing the Hessian for the molecule in solution.[20,21] $\tilde{P}^\lambda_{\alpha\beta}$ is obtained as

$$\tilde{P}^\lambda_{\alpha\beta} = \left(\frac{\partial\langle\psi^{sol}_g|(\tilde{\mu}^e_{el})_\beta|\psi^{sol}_g\rangle}{\partial X_{\lambda\alpha}}\right)_{\mathbf{r}_0{}^{sol}} + \frac{\partial\tilde{\mu}^N_{el}}{\partial X_{\lambda\alpha}} \tag{15}$$

The calculation of this term is performed by defining an

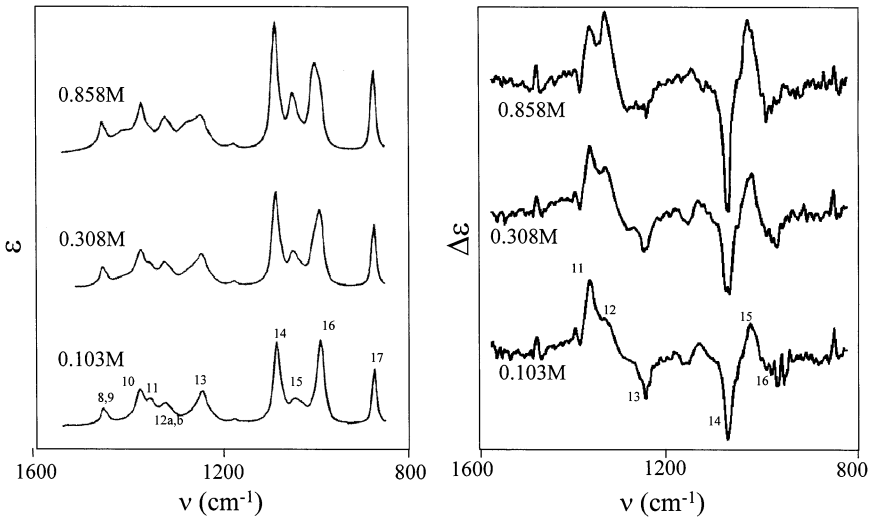

Figure 1. Experimental IR (left) and VCD (right) spectra of (*S*)-(−)-3-butyn-2-ol in CCl_4 solution at different concentrations. See ref 2.

additional set of external field-induced charges $\mathbf{q}^M$ spread on the cavity surface: details on this point can be found in ref 19. To compute $(P^{\lambda}_{\alpha\beta})^{sol}$, $\tilde{P}^{\lambda}_{\alpha\beta}$ and $(M^{\lambda}_{\alpha\beta})^{sol}$ the derivative of the wave function in solution with respect to the nuclear displacement is needed; the computation of this term within the PCM−IEF framework has already been treated (see ref 20). Recently we have presented a methodology to account for vibrational nonequilibrium solvent effects on such derivative and on the normal modes of the molecule (i.e., on the $S^{sol}_{\lambda\alpha,i}$ matrix).[21] We remark that nonequilibrium effects arise since the solvent cannot instantaneously equilibrate to the charge distribution of the vibrating molecule.

If an incomplete solvent response to vibrational motions (vibrational nonequilibrium) is to be accounted for, two additional refinements have to be considered:

(1) The calculation of $(P^{\lambda}_{\alpha\beta})^{sol}$ and $\tilde{P}^{\lambda}_{\alpha\beta}$ requires the derivative of the wave function in solution with respect to nuclear displacements. The formulation of such quantity within vibrational nonequilibrium has been implicitly treated in ref 21.

(2) The effects of solvent vibrational nonequilibrium affect molecular frequencies and normal modes (i.e., the $S^{sol}_{\lambda\alpha,i}$ matrix in eqs 13 and 14).

The calculation of $(M^{\lambda}_{\alpha\beta})^{sol}$ requires the evaluation of the derivative of the wave function with respect to the magnetic field $(\partial\psi^{sol}_G/\partial B_\beta)$ (compare eq 9). In this article such quantity will be evaluated by exploiting the GIAO method, already formulated within the PCM framework:[22,23] the introduction of solvent effects is realized by adding solvent dependent terms in the Coupled Hartree−Fock or Kohn−Sham scheme of the isolated system.

3. 3-Butyn-2-ol: Predominant Conformations, Hydrogen Bonding and Their Consequences on the Prediction of IR and VCD Spectra

As already said in the Introduction, experimental IR and VCD spectra of (*S*)-3-butyn-2-ol in CCl_4 solution at different concentrations have been measured by Wang and Polavarapu.[2] The experimental spectra are reproduced in Figure 1 (a and b) with indication of the band numbering suggested by the authors. In Figure 1a,b, as well as in all the figures reported in the following, both IR and VCD intensities are in arbitrary units but with a scale that is the same for the various spectra in each figure.

The spectra, especially the VCD ones, show noticeable differences in going from dilute to concentrated solution. Such a behavior has been attributed to intermolecular hydrogen bond effects between 3-butyn-2-ol molecules in the concentrated solution.[2]

In the following, we will use the theory presented in ref 19 and in the previous section to calculate IR and VCD spectra of (*S*)-3-butyn-2-ol in CCl_4 solution and we will then compare calculated and experimental results.

For the theoretical prediction of spectra at different solute concentrations two aspects have to be considered:

(a) Changes in the concentration of the solution may cause modifications in the dielectric properties of the local environment surrounding the solute molecules.

(b) The solute may give origin to clusters made of two or more hydrogen bonded molecules; obviously, the clustering increases with the solute concentration.

In the following, with "aggregation effects", we shall indicate the combination of aspects (a) and (b): Aspect (b) is straightforwardly connected to the phenomenon of aggregation while aspect (a) requires some comments.

In principle, it is always true that the dielectric constant of a solution does not coincide with that of the pure solvent (here CCl_4). However, in our case, also the dielectric constant of the most concentrated solution, as calculated by means of the dielectric constants of the two components and of the molarity, is very similar to that of pure CCl_4. Despite this, a molecule forming an aggregate will still experience a local dielectric environment different from infinite dilution due to the presence of other molecules in the aggregate, being the limiting case the molecule in the pure liquid.

In our approach effects described in aspect (a) will be evaluated by considering two opposite cases: (1) an infinitely dilute solution, with the static and dynamic permittivity of pure CCl_4; (2) a solution with dielectric properties similar to the pure alcohol. With regard to the aspect related to clustering (see item b), we will redefine the solute as a dimer of (*S*)-3-butyn-2-ol molecules, possibly immersed in a continuum solvent.

3.1. Computational Details. All the calculations have been performed by using density functional theory (DFT) with the B3LYP hybrid functional and the 6-311+G(d,p) basis set. The reliability of DFT for VCD calculation has been widely assessed (see for example ref 12) and the 6-311+G(d,p) basis set is known to be adequate to describe hydrogen-bonded systems.[24] A development version of the Gaussian program[25] has been used for the calculations both in vacuo and in solution. The

TABLE 1: Calculated B3LYP/6-311+G(d,p) Frequencies in the Range of Interest, Absorption Intensities (km/mol), and Rotational Strengths (10^{-44}esu^2 cm^2) for the Three Conformations of 3-Butyn-2-ol in CCl_4

A			B			C		
$\tilde{\nu}$	$\epsilon(\tilde{\nu})$	R	$\tilde{\nu}$	$\epsilon(\tilde{\nu})$	R	$\tilde{\nu}$	$\epsilon(\tilde{\nu})$	R
926	47.39	−2.20	921	20.95	4.914	926	36.23	0.90
1028	13.50	6.02	1032	98.42	−11.96	1035	81.72	−22.58
1090	63.77	24.56	1085	19.30	−12.24	1080	9.09	48.21
1117	79.00	−21.57	1120	74.18	−66.67	1124	46.82	−29.52
1232	52.03	34.22	1267	11.67	17.89	1272	55.75	−79.06
1341	5.829	−18.30	1338	9.154	19.58	1358	16.13	5.58
1402	17.39	−24.87	1401	12.68	4.706	1382	28.86	82.92
1403	21.56	0.49	1407	45.03	−33.37	1408	13.22	5.94
1484	6.630	4.04	1484	10.34	1.356	1481	6.38	−6.42
1490	3.152	−5.58	1487	0.964	−1.162	1492	2.97	5.14

calculation of infrared and VCD spectra in solution has been performed using analytical derivative methods in the nonequilibrium framework.[21] The calculated data in CCl_4 solution have been obtained by using $\epsilon_0 = 2.228$ and $\epsilon_{opt} = 2.129$ for the static and the optical permittivities, respectively. To simulate the alcoholic solution, we have used the permittivity values of pure butan-2-ol: $\epsilon_0 = 15.8$ and $\epsilon_{opt} = 1.95$. The geometries of all the systems have been optimized in each phase. The cavity used is of molecular shape and built by interlocking spheres. For the monomers as well as the clusters, the methyl group is inside a single sphere of radius 2.4 Å. The other atoms are inside a sphere of radius 2.04 Å for carbon, 1.44 Å for hydrogen, and 1.824 Å for oxygen. Only the electrostatic component of the solute−solvent interaction is taken into account in the calculations.

3.2. IR and VCD Spectra: The Pure Continuum Approach. When one has the aim of theoretically predicting molecular properties of flexible molecules, the choice of the local minima structures on the PES to use in the modeling should be done with care. In the scheme below the three different conformations of (*S*)-3-butyn-2-ol are represented: following Wang and Polavarapu,[2] we shall indicate them as trans-acetylene conformation (**A**), *trans*-H conformation (**B**), and *trans*-methyl conformation (**C**):

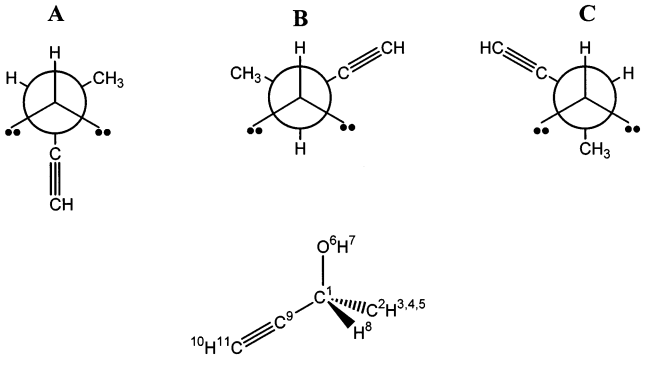

To obtain calculated spectra comparable with experimental ones, it is necessary to evaluate the statistical weight of each of the conformations. Once this has been done, calculated IR and VCD spectra are obtained as statistically averaged spectra of the single conformations.

Calculated vibrational frequencies, IR intensities, and rotational strengths of 3-butyn-2-ol in CCl_4 are reported in Table 1. The potential energy distribution (PED) analysis,[26] agrees with the findings previously reported by Wang and Polavarapu.

In Figures 2 and 3, calculated IR and VCD spectra for the three conformers in the range of frequencies of interest are shown. IR and VCD spectra have been drawn assuming Lorentzian line shapes (10 cm^{-1} of half-width), using calculated

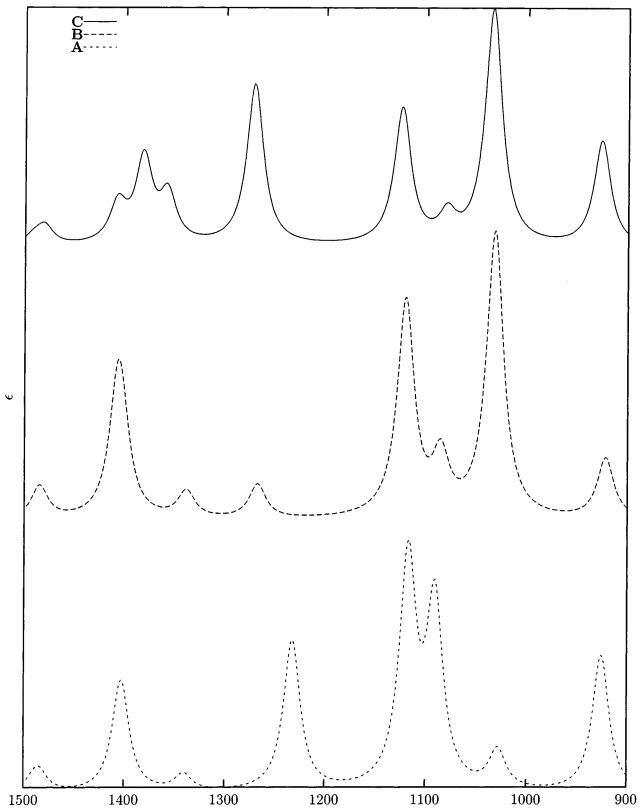

Figure 2. Calculated IR spectra for the three conformers. The spectra have been drawn assuming Lorentzian line shapes (10 cm^{-1} of half-width), using calculated frequencies and IR intensities.

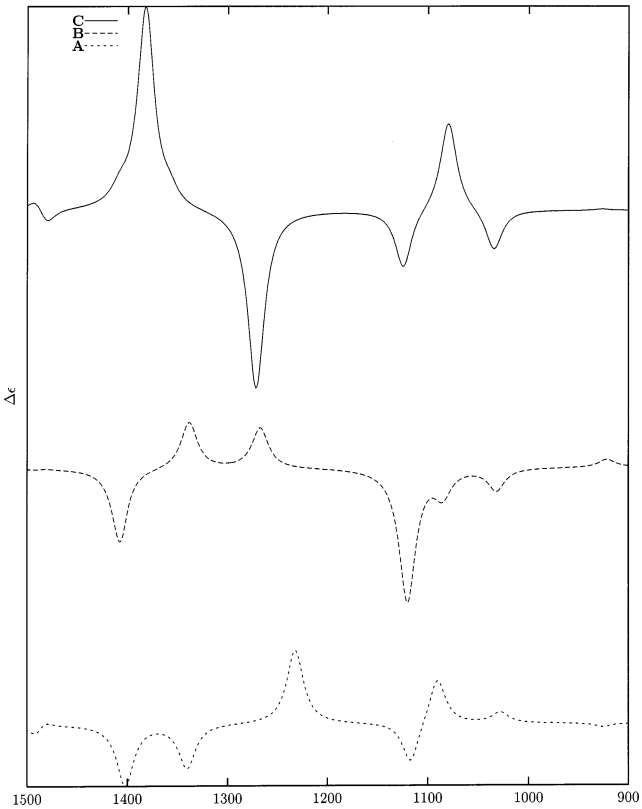

Figure 3. Calculated VCD spectra for the three conformers. The spectra have been drawn assuming Lorentzian line shapes (10 cm^{-1} of half-width), using calculated frequencies and rotational strengths.

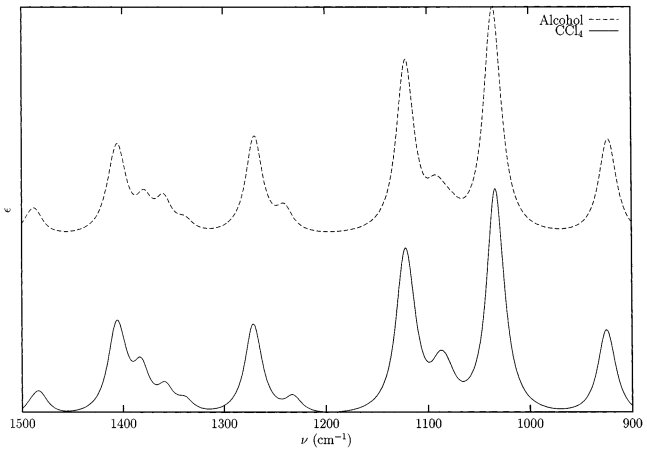

Figure 4. Population-weighted IR spectra in CCl_4 and in the hypothetical alcohol.

TABLE 2: Calculated B3LYP/6-311+G(d,p) Free Energies (G_{corr}) with Thermal and Zero-Point Corrections and Normalized Boltzmann Factors (b_{corr}) for the Three Conformations of 3-Butyn-2-ol in CCl_4

	G_{corr}	b_{corr}
A	−231.197561	0.1098
B	−231.198745	0.3849
C	−231.199002	0.5053

frequencies, IR intensities and rotational strengths. The scale for intensities (arbitrary units) is the same for the spectra of the three conformers.

From the inspection of Figures 2 and 3, we note that the spectra of the three conformers greatly differ from each other in the frequency and, in particular, in the intensity of the peaks. In the case of IR (Figure 2) large differences are noticed between **A** and the **B** and **C** conformations in the range between 1000 and 1150 cm^{-1}, while in the range between 1350 and 1450 cm^{-1} **C** shows a three-band structure which is absent in the spectra of **A** and **B**. Even more noticeable are differences between the VCD spectra of the three conformers (see Figure 3). In this case, not only do the three spectra differ in frequencies and intensities of the peaks but also the sign of the peaks changes in going from one conformation to another.

To proceed further and obtain calculated IR and VCD spectra of 3-butyn-2-ol in CCl_4 directly comparable with experimental ones (Figure 1), it is necessary to statistically average the calculated spectra of the various conformers according to their statistical weight. In Table 2, calculated PCM free energies of the three conformers in CCl_4 (including zero-point correction and thermal contributions at 298 K, as detailed in ref 15a), together with normalized Boltzmann factors, are reported.

To verify the effects of changes in the dielectric environment surrounding the molecule due to the variation in alcohol concentration, we have considered the case of a solvent with the same dielectric properties of the pure alcohol (see section above). The resulting IR and VCD spectra in CCl_4 and in the hypothetical alcohol are shown in Figures 4 and 5. We note that the Boltzmann factors for the second solvent do not significantly change with respect to CCl_4 and that the spectra of the single conformers, not reported here, remain similar but with differences in the relative intensities of the various peaks.

In Table 3, predicted frequencies extracted from the averaged IR spectrum in CCl_4 are reported in comparison with experimental values by Wang and Polavarapu.

Let us compare predicted and experimental IR and VCD spectra (Figures 4 and 5 with Figure 1).

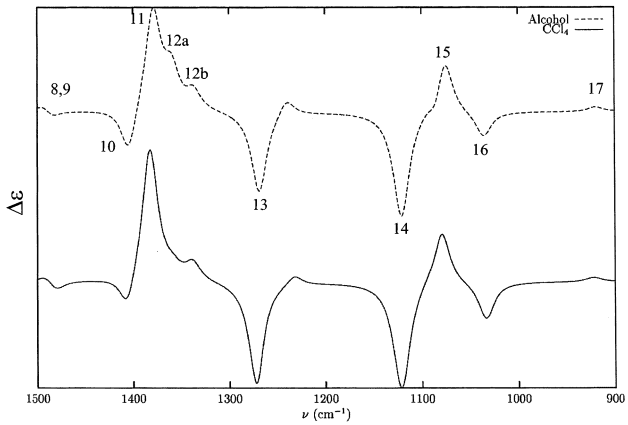

Figure 5. Population-weighted VCD spectra in CCl_4 and in the hypothetical alcohol.

TABLE 3: Calculated (Unscaled) B3LYP/6-311+G(d,p) and Observed Frequencies for 3-Butyn-2-ol in CCl_4[a]

band no.	exptl	calcd
8	1450	1484
10	1377	1406
11	1358	1383
12a	1329	1360
12b	1341	1341
13	1256	1271
14	1111	1122
15	1078	1086
16	1026	1033
17	922	926

[a] Experimental values were obtained by Wang and Polavarapu[2] from IR spectrum at concentration 0.103 M.

With regard to the calculated IR spectrum in CCl_4 (Figure 4), the overall agreement with the experimental one recorded by Wang and Polavarapu at low concentration (Figure 1) is very good. Looking at more refined details, the main differences between calculated and experimental spectra are that the relative intensities of bands 14, 16, and 17 are not reproduced well.

Passing to VCD spectra (Figures 1 and 5), we note a good agreement between the predicted spectrum in CCl_4 and the experimental one recorded at low concentration (the prediction of the sign of the peaks is very good). In particular, the structure of bands 11 and 13 is correctly predicted, as well as that of bands 14, 15, and 16, even if the intensity of the peak 14 is underestimated, similarly to what observed for IR.

Peak 12 is somewhat too low and too shifted at low frequency. Actually, it is composed of two transitions; one (12a) has a low intensity but the right frequency and gives rise to an asymmetry in the band 11. The other (12b) has a lower frequency and higher intensity. Although both can contribute to the experimental peak 12, 12a has a too low intensity to reproduce the experimental spectrum in the most dilute solution.

As expected, calculated IR and VCD spectra in CCl_4 do not match with the experimental spectra recorded at high concentration (Figure 1). In particular, in the predicted IR spectrum the asymmetry of the peak 16 is completely absent and the relative intensities of peaks 14, 15, and 16 are not very well reproduced. Passing to VCD, the structure in the range between 1200 and 1400 cm^{-1}, which is the region showing the largest changes with respect to the dilute case, is not well reproduced. A large underestimation of the relative intensity of peak 14, which greatly increases as the concentration of the alcohol increases, can also be noticed.

As reported above, to improve the description at high concentration, we have to consider effects due to aggregation.

Here in particular we focus on one of the two aspects of this phenomenon we have described before, namely the changes in the dielectric properties of the environment surrounding the solute molecules. To maximize such effects, we exploit an hypothetical solvent with characteristics similar to the pure alcohol.

As we can see from Figure 4, the IR spectrum is not very sensitive to the change in the dielectric environment: the only notable difference between spectra computed in CCl_4 and in the hypothetical alcohol is the decrease of the peak 11. Experimental spectra show a similar behavior as increasing the alcohol concentration. Passing to VCD (Figure 5), the main difference between the in-alcohol and in-CCl_4 spectrum is the intensity of the peak 12a, which is almost invisible in the CCl_4 spectrum, while it is a well visible shoulder in alcohol. This variation reproduces the experimental trend in passing from dilute to concentrated solutions, even if the calculated relative intensity of the 12a peak remains too low also in alcohol. We note that, from the comparison between in-CCl_4 and in-alcohol spectra, it appears that such a change, which is one of the most evident in the experimental spectra, can be in part assigned to the variations in the dielectric environment as the alcohol concentration is changed (this point will be reconsidered in the following section).

Finally, we observe that, according to the experimental behavior, the relative intensity of the peak 13 is slightly reduced compared to the CCl_4 solution, even if the observed reduction is more evident than the calculated one. There are no other significative changes in passing from the CCl_4 to the alcohol environment.

3.3. IR and VCD Spectra: The Mixed Continuum/Discrete Approach. The differences in IR and VCD spectra going from dilute to concentrated CCl_4 solution have been attributed by Wang and Polavarapu to intermolecular hydrogen bond effects between 3-butyn-2-ol molecules in the concentrated solution. To investigate this point a specific strategy will be followed: to take into account effects due to possible hydrogen bonding between alcohol molecules we introduce dimers. In addition, to separate the effects due to H-bonding from that induced by the dielectric environment, we consider three sets of dimers, with geometries and spectra calculated in vacuo, in CCl_4, and in the hypothetical alcohol, respectively.

In principle all possible dimers between **A**, **B**, and **C** should be considered; however, we have found that the dimers including **A** have a very low statistical weight (at least an order of magnitude smaller) with respect to the others (this reflects the low statistical weight observed for the **A** conformation; see Table 2). For this reason we will only consider dimers composed by 3- butyn-2-ol in the **C** or **B** conformations:

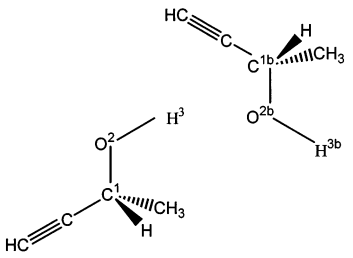

The resulting dimers are of four types according to all the possible combinations of **C** and **B** conformers; these will be indicated as **CC**, **BB**, **BC1**, and **BC2** dimers (see Figure 6).

Notice that the difference between the **BC1** and **BC2** dimers is that in **BC1** the **B** subunits acts as the H-donor, whereas in **BC2** the **C** subunit is the H-donor.

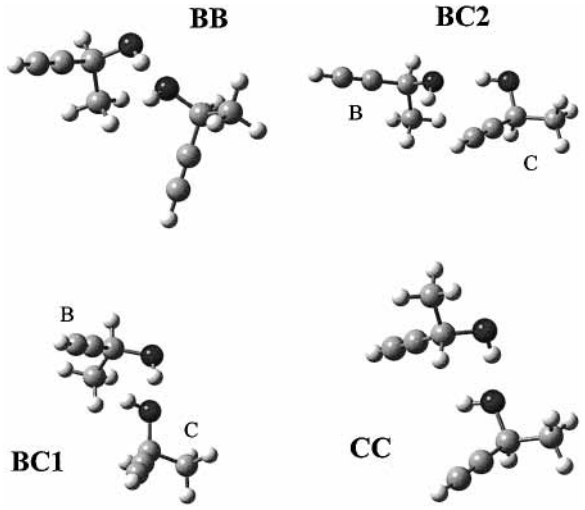

Figure 6. Structure of the four different dimers of 3-butyn-2-ol considered in this paper.

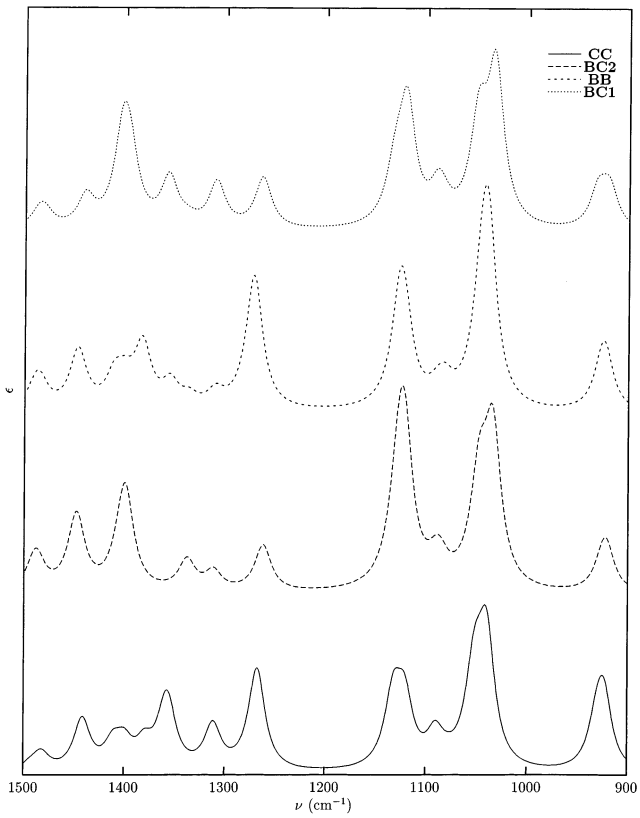

Figure 7. Calculated IR spectra corresponding to the four dimers in CCl_4.

In Figures 7 and 8, we report IR and VCD spectra corresponding to the four dimers, while in Figures 9 and 10, we report IR and VCD spectra obtained as their Boltzmann average (the free energy of each dimer and the corresponding normalized Boltzmann factors are reported in Table 4).

The spectra of the four dimers are reported only for the CCl_4 environment.

The four spectra of the single dimers show noticeable differences between one another. In particular, the frequency of the peaks is similar in the various cases but the intensities change remarkably. In the case of VCD (Figure 8) also the sign of the bands changes in passing from a dimer to another.

Let us now move to consider the averaged spectra in the various environments.

TABLE 4: Calculated B3LYP/6-311+G(d,p) Free Energies with Thermal and Zero-Point Corrections and Normalized Boltzmann Factors (b_{corr}) for the Four Dimers of 3-Butyn-2-ol in Vacuo, in CCl_4, and in Alcohol

	vac		CCl_4		alcohol	
	G_{corr}	b_{corr}	G_{corr}	b_{corr}	G_{corr}	b_{corr}
BB	−462.381895	0.0821	−462.382165	0.1443	−462.388835	0.1111
BC1	−462.382470	0.1510	−462.382304	0.1679	−462.389119	0.1690
BC2	−462.383453	0.4277	−462.382752	0.2690	−462.389885	0.3621
CC	−462.383234	0.3392	−462.383171	0.4193	−462.3898737	0.3578

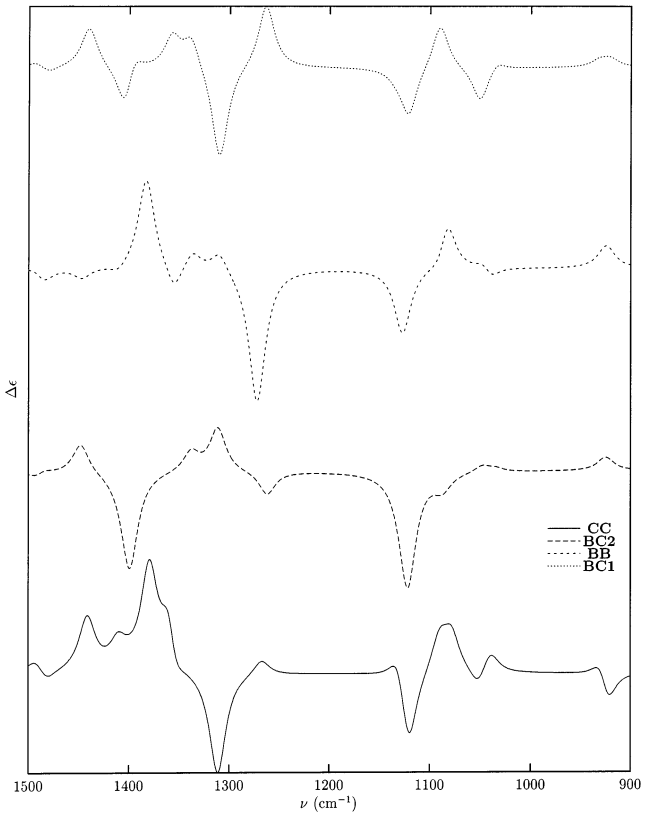

Figure 8. Calculated VCD spectra corresponding to the four dimers in CCl_4.

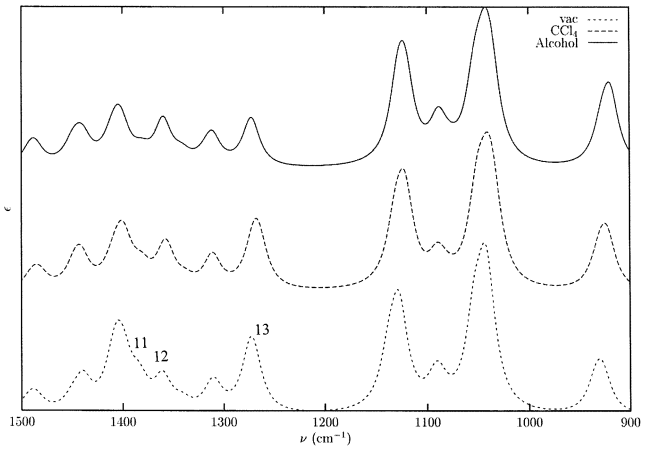

Figure 9. Population-weighted IR spectra of the four dimers in vacuo, in CCl_4, and in the hypothetical alcohol.

The analysis of the averaged IR spectrum (range 900−1200 cm^{-1}) in vacuo (Figure 9) shows that the agreement with respect to the experimental spectrum at high concentration cannot be improved by simply taking into account H-bond effects only. By comparing the calculated spectrum in vacuo with that resulting as superposition of the monomers (Figure 4), it results that H-bonding effects are responsible for the appearance of

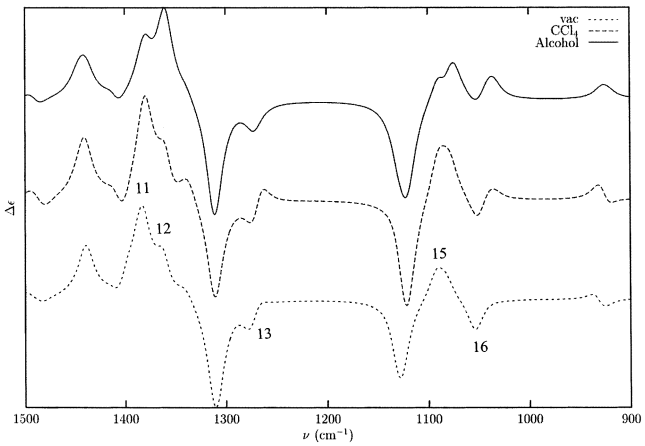

Figure 10. Population-weighted VCD spectra of the four dimers in vacuo, in CCl_4, and in the hypothetical alcohol.

two new peaks in the region 1200−1450 cm^{-1}, one at 1311 cm^{-1} and the other at 1440 cm^{-1}. The PED analysis shows that they both involve the bending of the $C^1O^2H^3$ angle. These two new peaks can be identified as the shoulders at around 1300 and 1410 cm^{-1} which appear in the 0.858 M experimental spectrum. By changing the dielectric environment of the dimers, the main modifications in the IR spectrum regard peaks 11 and 13 whose relative intensities decrease passing from vacuum to CCl_4 and to alcohol. This well reproduces the experimental trend as a function of the alcohol concentration.

Passing to VCD, we recall that the spectra calculated in the previous section with the pure continuum approach (Figure 5) have shown to be in disagreement with experiments at high concentration in three main aspects: (1) the relative intensity of the peak 12 is underestimated, even if the trend is correctly reproduced; (2) neither the relative intensity of the band 13 nor its trend are correctly reproduced; (3) the trend of the relative intensity of the peak 14 (which experimentally increases—in modulus—at higher concentration) is not well predicted. As for IR, we try to improve the description by introducing the VCD spectrum of dimers.

Let us start this analysis from the spectrum calculated in vacuo (Figure 10), which is representative of H-bond effects only.

(1) Peak 12a is now visible as a shoulder of peak 11. Thus, the presence of clustering enhances the intensity of this peak. Noticeably, the normal mode of the vibration originating peak 12a has small projections on the internal coordinates involving the H-bond atoms.

(2) The pure continuum approach (Figure 5) gives only one negative peak in the region of the experimental 13 peak. The cluster approach gives instead two negative peaks: one (small) at the same frequency of the peak obtained with the pure continuum and the other (larger) at a slightly higher frequency. From the analysis of the spectra of the conformers, we see that these two bands can be attributed to the bending of the COH angle. In particular, the band at lower frequency is caused by the bending of the H-acceptor COH group ($C^{1b}O^{2b}H^{3b}$ in the

scheme above) of the **B** and **C** subunits; this mode is VCD-active in all the four dimers. On the other hand, the band at higher frequency is caused by the bending of the H-donor $C^1O^2H^3$ group of the **C** subunit; this mode is present in the **CC** and **BC2** dimers only. The presence of two bands in this region is compatible with the experimental spectra. From such spectra, it seems that an increase in concentration (and thus in aggregation) decreases the intensity of the band at lower frequency and increases the modulus of the intensity of the new negative band at a frequency between 12 and 13, which is not visible in the most diluted spectrum.

(3) The relative intensity of the peak 14 is slightly affected by the aggregation and its trend remains thus unexplained.

The calculated VCD spectrum for the dimers in vacuo (Figure 10) also shows a peak at 1440 cm^{-1}, which is not present in the calculated spectrum for the monomers and is the equivalent of the IR peak which we have discussed previously. The experimental spectra in that region is quite noisy, and thus it is not easy to detect peaks there: nevertheless, the predicted intensity of the peak at 1440 cm^{-1} seems not to be compatible with the experiment.

By introducing the dielectric constant effect, i.e., by passing from vacuum to CCl_4 and to alcohol, we observe two important changes.

The structure of the spectrum near peaks 15 and 16 becomes more complex: a positive peak arises and peak 15 splits, decreasing its intensity. The appearance of the positive peak can be attributed to an increase in the intensities of peaks (intensities which are very low for dimers in vacuo) of all the conformers. The most important change, however, regards the relative intensities of peaks 11 and 12, which reverse in passing from vacuum and CCl_4 to alcohol. This reproduces the experimental behavior in passing from dilute to concentrated solution.

The comparison between the intensities of peaks 11 and 12 computed for the dimers in the gas phase and in alcohol solution, together with the same comparison on the monomers, shows that both clustering and local dielectric environment effects are to be invoked to explain the experimentally observed relative intensity of the two bands at various concentrations. In fact neither the clustering alone (see "vac" spectrum in Figure 10) nor the dielectric effects alone (see "alcohol" spectrum in Figure 5) can reproduce the experimental findings of the increase of peak 12 intensity from dilute to concentrated solutions.

Our results allow us to explore in depth the conclusions made by Wang and Polavarapu to explain modifications of the IR and VCD spectra as a function of the alcohol concentration in terms of changes in conformation weights. Our approach in fact makes it possible to directly evaluate the changes in the Boltzmann weights of the conformers due to clustering and dielectric environment effects. In addition, we have explicitly calculated the spectra of single conformers of both nonaggregated and aggregated systems in various dielectric environments (from gas-phase to liquid alcohol). The spectra of the four dimers reported in Figure 8 are not simply the superposition of the spectra of the corresponding **B** and **C** conformers (see Figure 3): this shows that clustering gives origin to specific VCD patterns (see, for example, the structured shape of the peak around 1400 cm^{-1} in the spectrum of the **CC** dimer, which is only slightly visible in the spectrum of the C conformer). In addition, from the data reported in Table 4 for the four dimers we can extract a relative population of **B** and **C** of 36% and 64% (when calculated in CCl_4); the corresponding values of the nonaggregated systems (see Table 2) are 43% and 57% (neglecting the **A** conformer), respectively. This variation alone does not explain the significant differences of the observed spectra at different concentrations.

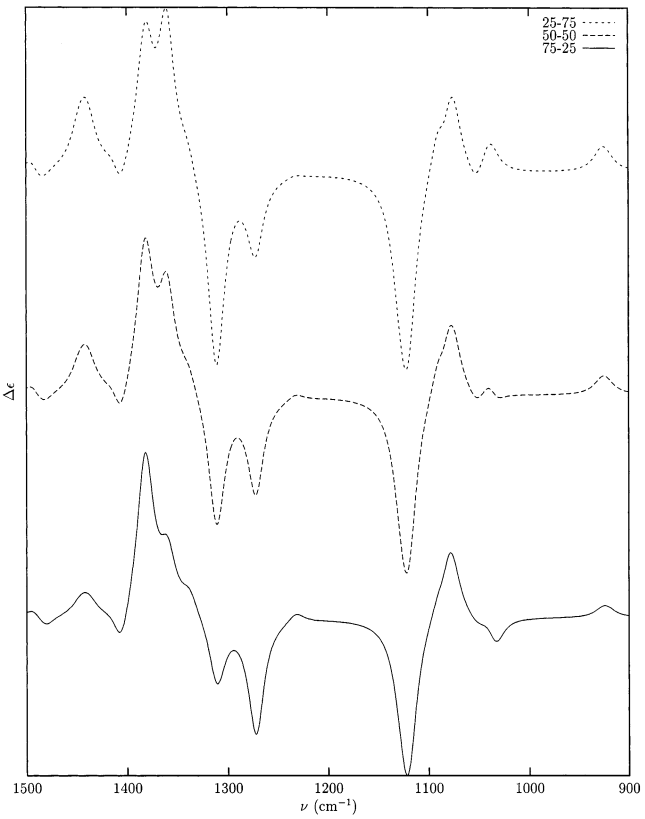

Figure 11. VCD spectra resulting from a combination of the spectra of monomers in CCl_4 and dimers in alcohol, obtained introducing three different arbitrary weights corresponding to 75:25, 50:50, and 25:75 percentages of monomers and dimers, respectively.

The analysis reported so far has been focused on the spectra of the monomers and dimers separately; however, the experimental spectra at different concentrations are clearly a superposition of both monomers and aggregates. The correct way of reproducing them would be to calculate thermodynamic constants for all possible aggregation equilibria and to use them to evaluate the concentration of each species. This, however, would require inclusion of clusters larger than dimers and the necessity of computing accurate aggregation energies with consideration, for example, of the effects of the basis set superposition error (BSSE).[28] In addition, the contributions to the equilibrium constant due to translation and rotation motions for the solvated systems should be accurately determined in order to get reliable data. Such kind of analysis requires a computational effort which would lead too far from the main scope of the present paper. Here, we thus limit ourselves to present a more qualitative approach, showing the VCD spectra which result from a combination of the spectra of monomers and dimers, obtained introducing three different arbitrary weights corresponding to 75:25, 50:50, and 25:75 percentages of monomers and dimers, respectively (see Figure 11). In particular, we have chosen the monomers in CCl_4 and the dimers in the hypothetical alcohol as the two limit cases to be combined.

Above, we have analyzed in details the changes in the VCD spectrum in passing from the monomers to the dimers and from a dielectric environment to another; here, we only make a further remark. The three different spectra obtained with different weights of single conformers and dimers confirm not only that the observed spectra are always a superposition of different

contributions but also that, by combining the effects of clustering with those induced by the dielectric environment, we can understand and reproduce the trend observed in the experimental spectra at different concentrations.

4. Summary and Conclusions

In this paper we have presented the theory of VCD in solution within the PCM framework including local field and nonequilibrium effects. This theory has been applied to the study of (*S*)-3-butyn-2-ol in CCl_4 solution. Experimental IR and VCD spectra of (−)-3-butyn-2-ol in CCl_4 solution at different concentrations have been measured by Wang and Polavarapu.[2] The spectra, especially the VCD ones, show noticeable differences in going from dilute to concentrated solutions. From the theoretical point of view the simulation of IR and VCD spectra of this system and, even more important, the correct description of changes with changing concentration, represents a challenging problem from different points of view. First of all, the solute may exist in three different conformations which are differently stabilized by the solvent: the IR and VCD spectra have thus to be obtained by adding population-weighted spectra of all conformers. In addition, to describe the changes of spectra at different solute concentrations, two further aspects have to be considered: (a) possible modifications in the dielectric properties of the local environment surrounding the solute molecules due to changes in the concentration of the solution; (b) the formation of possible clusters made of two or more hydrogen bonded molecules of the solute. These two effects have been explicitly introduced in the theoretical model by computing the VCD spectra of the conformers and of the possible dimers in two different dielectric environments: CCl_4 and an hypothetical dielectric medium with macroscopic characteristics of the pure alcohol.

Regarding the formation of clusters (point b), we remark that larger systems made of more than two alcohol molecules can be formed; spectroscopic studies on similar alcohols (butan-1-ol and butan-2-ol), in fact, seem to show that the average association number ranges from 2 to 4.[27] In this work we have explicitly treated only dimers due to the high computational effort needed to account for larger clusters. However, we note that the effects of such structures can be partially recovered by introducing a dielectric environment which presents the same features of the pure alcohol. In this way, in fact, the continuum dielectric qualitatively simulate the effects due to the alcohol molecules of the clusters which we have not explicitly included in the calculations. Moreover, we can assume that at high concentrations weak interacting aggregates of many alcohol molecules are formed in addition to H-bonded clusters: this situation, once again, can give origin to local dielectric environments between the pure alcohol and the solution. The validity of this modeling is confirmed by the good agreement between calculated and experimental spectra at increasing concentration when dielectric effects are taken into account in addition to H-bonding.

Supporting Information Available: Tables of calculated geometrical parameters for 3-butyn-2-ol and its dimers and calculated frequencies for dimers of 3-butyn-2-ol. This material is available free of charge via the Internet at http://pubs.acs.org.

References and Notes

(1) Toda, F. Jpn. Kokai Tokkyo Koho A2 1987, 27 (patent JP6224653); *Chem. Abstr.* **1987**, *108*, 204218.

(2) Wang, F.; Polavarapu, P. L. *J. Phys. Chem. A* **2000**, *104*, 1822.

(3) (a) Miertuš, S.; Scrocco, E.; Tomasi, *J. Chem. Phys.* **1981**, *55*, 117; (b) Cammi, R.; Tomasi, J. J. *Comp. Chem.* **1995**, *16*, 1449.

(4) (a) Tomasi, J.; Cammi, R.; Mennucci, B. *Int. J. Quantum Chem.* **1999**, *75*, 783. (b) Mennucci, B., Cammi, R.; Tomasi, J. *Int. J. Quantum Chem.* **1999**, *75*, 767.

(5) Gontrani, L.; Mennucci, B.; Tomasi, J. *J. Mol. Struct. (THEOCHEM)* **2000**, *500*, 113.

(6) (a) Aamouche, A.; Devlin, F. J.; Stephens, P. J. *J. Am. Chem. Soc.* **2000**, *122*, 2346. (b) Zhao, C.; Polavarapu, P. L.; Grosenick, H.; Schurig, V. *J. Mol. Struct.* **2000**, *550*, 105. (c) Aamouche, A.; Devlin, F. J.; Stephens, P. J.; Drabowicz, J.; Bujnicki, B.; Mikolajczyk, M. *Chem.—Eur. J.* **2000**, *6*, 4479. (d) Wang, F.; Polavarapu, P. L. *J. Phys. Chem. A* **2000**, *104*, 10683. (e) Stephens, P. J.; Aamouche, A.; Devlin, F. J.; Superchi, S.; Donnoli, M. I.; Rosini, C. *J. Org. Chem.* **2001**, *66*, 3671. (f) Devlin, F. J.; Stephens, P. J.; Scafato, P.; Superchi, S.; Rosini, C. *Tetrahedron Asym.* **2001**, *12*, 1551. (g) Bohr, H. G.; Frimand, K.; Jalkanen, K. J.; Nieminen, R. M.; Suhai, S. *Phys. Rev. E* **2001**, *6402*, 1905. (h) Wang. F.; Polavarapu, P. L. *J. Phys. Chem. A* **2001**, *105*, 6991.

(7) (a) Han, W. G.; Jalkanen, K. J.; Elstner, M.; Suhai, S. *J. Phys. Chem. B.* **1998**, *102*, 2587. (b) Tajkhorshid, E.; Jalkanen, K. J.; Suhai, S. *J. Phys. Chem. B* **1998**, *102*, 5899. (c) Frimand, K.; Bohr, H.; Jalkanen, K. J.; Suhai, S. *Chem. Phys.* **2000**, *255*, 165.

(8) (a) Amos, R. D. *Adv. Chem. Phys*. **1987**, *67*, 99. (b) Pulay, P. *Adv. Chem. Phys*. **1987**, *67*, 99. (c) Johnson, B. G.; Frisch, M. J. *J. Chem. Phys.* **1994**, *100*, 7429.

(9) Bak, K. L.; Jorgensen, P.; Helgaker, T.; Ruud, K.; Jensen, H. J. Aa. *J. Chem. Phys.* (a) **1993**, *98*, 8873; (b) **1994**, *100*, 6620.

(10) Cheesman, J. R.; Frisch, M. J.; Devlin, F. J.; Stephens, P. *J. Chem. Phys. Lett.* **1996**, *252*, 211.

(11) (a) London, F. *J. Phys. Radium (Paris)* **1937**, *8*, 397. (b) Ditchfield, R. *Mol. Phys.* **1974**, *27*, 789.

(12) (a) Stephens, P. J.; Devlin, F. J.; Ashvar, C. S.; Chabalowski, C. F.; Frisch, M. J. *Faraday Discuss*. **1994**, *99*, 103. (b) Stephens, P. J.; Devlin, F. J.; Chabalowski, C. F.; Frisch, M. J. *J. Phys. Chem.* **1994**, *98*, 11623. (c) Devlin, F. J.; Stephens, P. J.; Cheeseman, J. R.; Frisch, M. J. *J. Phys. Chem. A* **1997**, *101*, 6322. Devlin, F. J.; Stephens, P. J.; Cheeseman, J. R.; Frisch, M. J. *J. Phys. Chem. A* **1997**, *101*, 9912.

(13) Brown, W. F. in *Encyclopedia of Physics*; Flügge, S., Ed.; Springer: Berlin, 1956.

(14) (a) Böttcher, C. J. F. *Theory of Electric Polarization*; Elsevier: Amsterdam, 1973; vol. I. (b) Böttcher, C. J. F.; Bordewijk, P. *Theory of Electric Polarization*; Elsevier: Amsterdam, 1978; Vol. II.

(15) (a) Tomasi, J.; Persico, M. *Chem. Rev.* **1994**, *94*, 2027. (b) Cramer, C. J.; Truhlar, D. G. *Chem. Rev.* **1999**, *99*, 2161.

(16) Stephens, P. J. *J. Phys. Chem.* (a) **1985**, *89*, 748; (b) **1987**, *91*, 1712.

(17) (a) Cancès, E.; Mennucci, B. *J. Math. Chem.* **1998**, *23*, 309. (b) Cancès, E.; Mennucci, B.; Tomasi, J. *J. Chem. Phys.* **1997**, *107*, 3031. (c) Mennucci, B.; Cancès, E.; Tomasi, J. *J. Phys. Chem. B* **1997**, *101*, 10506.

(18) Mennucci, B.; Cammi, R.; Tomasi, J. *J. Chem. Phys.* **1998**, *109*, 2798.

(19) Cammi, R.; Cappelli, C.; Corni, S.; Tomasi, J. *J. Phys. Chem. A* **2000**, *104*, 9874.

(20) (a) Cancès, E.; Mennucci, B. *J. Chem. Phys.* **1998**, *109*, 249. (b) Cancès, E.; Mennucci, B.; Tomasi, J. *J. Chem. Phys.* **1998**, *109*, 260, for the first derivative. (c) Mennucci, B.; Cammi, R.; Tomasi, J. *J. Chem. Phys.* **1999**, *110*, 6858, for the second derivatives.

(21) Cappelli, C.; Corni, S.; Cammi, R.; Mennucci, B.; Tomasi, J. *J. Chem. Phys.* **2000**, *113*, 11270.

(22) Cammi, R. *J. Chem. Phys.* **1998**, *109*, 3185.

(23) Cammi, R.; Mennucci, B.; Tomasi, J. *J. Chem. Phys.* **1999**, *110*, 7627.

(24) Rablen, P. R.; Lockman, J. W.; Jorgensen, W. L. *J. Phys. Chem. A* **1998**, *102*, 3782.

(25) Frisch, M. J.; Trucks, G. W.; Schlegel, H. B.; Scuseria, G. E.; Robb, M. A.; Cheeseman, J. R.; Zakrzewski, V. G.; Montgomery, J. A., Jr.; Stratmann, R. E.; Burant, J. C.; Dapprich, S.; Millam, J. M.; Daniels, A. D.; Kudin, K. N.; Strain, M. C.; Farkas, O.; Tomasi, J.; Barone, V.; Cossi, M.; Cammi, R.; Mennucci, B.; Pomelli, C.; Adamo, C.; Clifford, S.; Ochterski, J.; Petersson, G. A.; Ayala, P. Y.; Cui, Q.; Morokuma, K.; Malick, D. K.; Rabuck, A. D.; Raghavachari, K.; Foresman, J. B.; Ortiz, J. V.; Baboul, A. G.; Cioslowski, J.; Stefanov, B. B.; Liu, G.; Liashenko, A.; Piskorz, P.; Komaromi, I.; Gomperts, R.; Martin, R. L.; Fox, D. J.; Keith, T.; Al−Laham, M. A.; Peng, C. Y.; Nanayakkara, A.; Challacombe, M.; Gill, P. M. W.; Johnson, B.; Chen, W.; Wong, M. W.; Andres, J. L.; Gonzalez, C.; Head-Gordon, M.; Replogle, E. S.; Pople, J. A. Gaussian 01, Development Version (Revision B.01); Gaussian, Inc., Pittsburgh PA., 2001.

(26) Martin, J. M. L.; Van Alsenoy, C. GAR2PED (University of Antwerp, 1995).

(27) Iwahashi, M.; Suzuki, M.; Katayama, N.; Matsuzawa, H.; Czarnecki, M. A.; Ozaki, Y.; Warisaka, A. *Appl. Spectrosc*. **2000**, *54*, 268.

(28) Weinhold, F. *J. Chem. Phys.* **1998**, *109*, 367.